The Astrophysical Journal, 628:973–985, 2005 August 1

THE EFFECTIVE TEMPERATURE SCALE OF GALACTIC RED SUPERGIANTS: COOL, BUT NOT AS COOL AS WE THOUGHT

Emily M. Levesque[1,2] and Philip Massey[2]
Lowell Observatory, 1400 West Mars Hill Road, Flagstaff, AZ 86001; e_levesq@space.mit.edu, phil.massey@lowell.edu
K. A. G. Olsen[3]
Cerro Tololo Inter-American Observatory, National Optical Astronomy Observatory, Casilla 603, La Serena, Chile; kolsen@noao.edu
Bertrand Plez and Eric Josselin
Groupe de Recherche en Astronomie et Astrophysique du Languedoc, Université de Montpellier II, 34095 Montpellier Cedex 05, France; bertrand.plez@graal.univ-montp2.fr, eric.josselin@graal.univ-montp2.fr
and
Andre Maeder and Georges Meynet
Geneva Observatory, 1290 Sauverny, Switzerland; andre.maeder@obs.unige.ch, georges.meynet@obs.unige.ch
Received 2004 November 18; accepted 2005 April 12

ABSTRACT

We use moderate-resolution optical spectrophotometry and the new MARCS stellar atmosphere models to determine the effective temperatures of 74 Galactic red supergiants (RSGs). The stars are mostly members of OB associations or clusters with known distances, allowing a critical comparison with modern stellar evolutionary tracks. We find we can achieve excellent matches between the observations and the reddened model fluxes and molecular transitions, although the atomic lines Ca I λ4226 and Ca II H and K are found to be unrealistically strong in the models. Our new effective temperature scale is significantly warmer than those in the literature, with the differences amounting to 400 K for the latest type M supergiants (i.e., M5 I). We show that the newly derived temperatures and bolometric corrections give much better agreement with stellar evolutionary tracks. This agreement provides a completely independent verification of our new temperature scale. The combination of effective temperature and bolometric luminosities allows us to calculate stellar radii; the coolest and most luminous stars (KW Sgr, Case 75, KY Cyg, HD 206936 = μ Cep) have radii of roughly 1500 $R_\odot$ (7 AU), in excellent accordance with the largest stellar radii predicted from current evolutionary theory, although smaller than that found by others for the binary VV Cep and for the peculiar star VY CMa. We find that similar results are obtained for the effective temperatures and bolometric luminosities using only the dereddened $V-K$ colors, providing a powerful demonstration of the self-consistency of the MARCS models.

Subject headings: dust, extinction — stars: atmospheres — stars: fundamental parameters — stars: late-type — supergiants

Online material: extended figure set

1. INTRODUCTION

Red supergiants (RSGs) are an important but poorly characterized phase in the evolution of massive stars. As discussed recently by Massey (2003) and Massey & Olsen (2003), stellar evolution models do not produce RSGs that are as cool or as luminous as those observed. Such a discrepancy is not surprising, given the tremendous challenge RSGs present to evolutionary calculations. The RSG opacities are uncertain because of possible deficiencies in our knowledge of molecular opacities. The atmospheres of these stars are highly extended, but in general the models assume plane-parallel geometry. In addition, the velocities of the convective layers are nearly sonic, and even supersonic in the atmospheric layers, giving rise to shocks (Freytag et al. 2002). This invalidates the mixing-length assumptions, making the star's photosphere very asymmetric and its radius poorly defined, as demonstrated by recent high angular resolution observations of Betelgeuse (Young et al. 2000).

While considering these challenges, we must, however, recognize that the "observed" location of RSGs in the H-R diagram is also highly uncertain, as it requires a sound knowledge of the effective temperatures of these stars. For stars this cool (roughly 3000–4000 K), the bolometric corrections (BCs) are quite significant (-4 to -1 mag), and these BCs are a steep function of effective temperature. This makes an accurate effective temperature scale doubly necessary, as a 10% error in $T_{\rm eff}$ would lead to a factor of 2 error in bolometric luminosity computed from V, according to the Kurucz (1992) model atmospheres as described by Massey & Olsen (2003). While interferometric data have provided a good fundamental calibration of red *giants* (see, for example, Dyck et al. 1996), there are not enough nearby RSGs to employ this method in determining an effective temperature scale. Instead, previous scales have relied on using broadband colors to assign temperatures based on the few RSGs with measured diameters (Lee 1970, following Johnson 1964, 1966), or on "observed" BCs (from infrared [IR] measurements) combined with the assumption of a blackbody distribution for the continuum (see Flower 1975, 1977). However, $(B-V)_0$ is highly sensitive to the surface gravity of the star due to the increased

[1] Participant, Research Experiences for Undergraduates program, Summer 2004; current address: Massachusetts Institute of Technology, 77 Massachusetts Avenue, Cambridge, MA 02139.

[2] Visiting Astronomer, Kitt Peak National Observatory (KPNO), National Optical Astronomy Observatory (NOAO), which is operated by the Association of Universities for Research in Astronomy (AURA), Inc., under cooperative agreement with the National Science Foundation (NSF).

[3] Visiting Astronomer, Cerro Tololo Inter-American Observatory (CTIO), NOAO, which is operated by AURA, Inc., under cooperative agreement with the NSF.

effects of line blanketing with lower surface gravities; the effect is particularly pronounced at B due to the multitude of weak metal lines in the region (see discussion in Massey 1998). In point of fact, the true continuum at these temperatures (that produced by continuous absorption) is probably never seen, as noted by Aller (1960). White & Wing (1978) attempt to get around this problem by a novel scheme involving an eight color narrowband filter set, which was fit by a blackbody curve and iteratively corrected to determine uncontaminated continua. However, in all such continuum fits there is always some degeneracy between changes in the effective temperature and changes in the amount of reddening to be applied to the models; this is particularly important for the RSGs, as they can be heavily reddened.

An alternative approach would be to make use of the incredibly rich TiO molecular bands that dominate the optical spectra of M-type stars. Atmospheric models, however, have not always included an accurate opacity, especially for molecular transitions. The problem largely stems from the fact that any molecule found in a stellar atmosphere—even that of an M-type star—must be considered "high temperature," while most laboratory data have been obtained at much lower temperatures and do not include high-excitation transitions. The situation has decidedly improved in the past years, in large part due to the great efforts by a few groups to compute ab initio line lists (e.g., Partridge & Schwenke 1997; Harris et al. 2002), and it now seems quite satisfactory regarding oxygen-rich mixtures, such as TiO (see reviews by Gustafsson & Jorgensen 1994 and Tsuji 1986).

The new generation of MARCS models (Gustafsson et al. 1975; Plez et al. 1992) now includes a much improved treatment of molecular opacity (see Plez 2003; Gustafsson et al. 2003). Using absolute spectrophotometry (both continuum fluxes and the strengths of the G band for K stars and the TiO bands for M stars), these models can now be used to make a far more robust determination of $T_{\rm eff}$ and the reddening. Since band strengths are used to determine the spectral type of RSGs, these new models could serve as a definitive connection between spectral type and $T_{\rm eff}$.

Here we present spectrophotometry of 74 Galactic K- and M-type supergiants (§ 2) and use fits of the MARCS models to determine effective temperatures (§ 3).[4] We begin the analysis by reclassifying the stars (§ 3.1) and then construct a new $T_{\rm eff}$ scale for Galactic RSGs (§ 3.2). Most of these stars are members of associations and clusters with known distances, allowing us to also place the stars on the H-R diagram for comparison with the latest generation of stellar evolutionary models, which include the effects of stellar rotation (§ 3.3). In § 3.4, we compare the physical parameters of these stars derived in the optical to those found from K-band photometry in order to test the self-consistency of the MARCS models.

In future work, we will extend this study to the lower metallicity Magellanic Clouds, where the distribution of spectral subtypes is considerably earlier than in the Milky Way (Elias et al. 1985; Massey & Olsen 2003). The lower abundance of TiO may by itself lead to a lower $T_{\rm eff}$ for stars of the same spectral subtype, as suggested by Massey & Olsen (2003).

2. OBSERVATIONS

2.1. *The Sample*

Our stars are listed in Table 1. The sample was selected in order to cover the full range of spectral subtypes from early K through the latest M supergiants. The sample was originally chosen to contain only stars with probable membership in OB associations and clusters with known distances (Humphreys 1978; Garmany & Stencel 1992), but we supplemented this list with spectral standards from the list of Morgan & Keenan (1973) in order to help refine the spectral classification. We indicate both cluster membership and/or use as a spectral standard in the table. The photometry comes from a variety of sources, as indicated; one should keep in mind that most (if not all) of these stars are variable at the level of several tenths of a magnitude or more in V. We have included the $V - K$ colors as well, where the K comes from Josselin et al. (2000) and references therein.

Distances of OB associations are notoriously uncertain, as most are far too distant for reliable trigonometric parallaxes; instead, spectral parallaxes need to be used, often resulting in a large dispersion due to the large scatter in M_V for a given spectral subtype (see Conti 1988). In Table 2, we give the distances from several sources, when possible, for each OB association or cluster in our sample; in general, the agreement is within a few tenths of a magnitude. We also include in Table 2 the "average" reddenings determined from the values for *early*-type members listed by Humphreys (1978) for the OB associations. For the clusters, we list the average reddening values given by Mermilliod & Paunzen (2003). We note that in general membership in an OB association is never perfectly well established, and therefore there is an additional uncertainty connected with the distance of any particular star.

2.2. *Spectrophotometry*

The spectrophotometry data were obtained during three observing runs: two with the KPNO 2.1 m telescope and GoldCam Spectrograph (2004 March 17–24 and May 28–June 1) and one with the CTIO 1.5 m telescope and Cassegrain CCD spectrometer (2004 March 7–12). Similar resolutions and wavelength coverage were obtained in both hemispheres. Detailed information on the observing parameters is given in Table 3.

The Kitt Peak observations were taken under sporadically cloudy conditions in March, while all of the nights in May/June were photometric. Before observing each object, the spectrograph was manually rotated so that the slit was aligned with the parallactic angle. We aimed for a signal-to-noise ratio (S/N) of 50 per spectral resolution element (4 pixels) at the bluest end of the spectrum, with care being taken not to saturate the detector at the reddest end. For the brightest stars ($V < 6$), we employed a 5.0 or 7.5 mag neutral density filter. Observations of the flat-field lamps were obtained both with and without these filters in order to correct for the wavelength dependence of the transmission of these "neutral" filters. Throughout each night we also observed a set of spectrophotometric standards. The seeing for these observations was $1\farcs2$–$3''$, with a typical value of $2''$. Exposures of both dome flats and projector flats were obtained at the beginning of each night; for the red nights, we also obtained projector flats throughout the night to monitor any shifting of the fringe pattern that affects the CCD at longer wavelengths. Wavelength calibration exposures of a He-Ne-Ar lamp were obtained at the beginning and end of each night.

At CTIO, it was not practical to always observe at the parallactic angle; instead, each star was observed with a single exposure through a very wide slit (for good relative fluxes), followed by a series of shorter exposures obtained through a narrow slit (for good resolution). Projector flats were obtained for all wavelength regions through both the wide and narrow slits. The exposures were typically obtained in conjunction with a wavelength calibration exposure, although in practice we found there was little

[4] We are making both the observed spectra and models available to others via data files at the Centre de Données Astronomiques de Strasbourg (CDS).

TABLE 1

Program Stars

			Photometry				Spectral Type			
Star	α_{2000}	δ_{2000}	V	$B-V$	$V-K$	Ref.[b]	Old[c]	New	OB Association[a]	Comment
BD +59°38	00 21 24.29	+59 57 11.2	9.13	2.49	. . .	1	M2 Iab	M2 I	Cas OB4	MZ Cas
Case 23	00 49 10.71[d]	+64 56 19.0[d]	10.72	2.77	7.80	2	M1 Iab	M3 I	Cas OB7	
HD 236697	01 19 53.62	+58 18 30.7	8.65	2.16	5.41	3	M2 Ib	M1.5 I	NGC 457	V466 Cas
BD +59°274	01 33 29.19	+60 38 48.2	8.55	2.09	5.24	1	M0 Ib	M1 I	Cas OB8/NGC 581	
BD +60°335	01 46 05.48	+60 59 36.7	9.15	2.34	. . .	1	M3 Iab	M4 I	Cas OB8/NGC 663	
HD 236871	01 47 00.01	+60 22 20.3	8.74	2.27	. . .	2	M3 Iab	M2 I	Cas OB8	
HD 236915	01 58 28.91	+59 16 08.7	8.30	2.20	. . .	2	M2 Iab	M2 I	Per OB1-A	
BD +59°372	01 59 39.66	+60 15 01.7	9.30	2.28	. . .	2	K5–M0 I	K5–M0 I	Per OB1-A	
BD +56°512	02 18 53.29	+57 25 16.7	9.23	2.47	6.99	1	M4 Ib	M3 I	Per OB1-D	BU Per
HD 14469[e]	02 22 06.89	+56 36 14.9	7.63	2.17	6.24	1	M3–M4 Iab	M3–M4 I	Per OB1-D	SU Per
HD 14488	02 22 24.30	+57 06 34.3	8.35	2.27	6.62	1	M4 Iab	M4 I	Per OB1-D/NGC 884	RS Per
HD 14528	02 22 51.72	+58 35 11.4	9.23	2.65	7.78	1	M4e I	M4.5 I	Per OB1-D	S Per
BD +56°595	02 23 11.03	+57 11 58.3	8.18	2.23	5.42	1	M0 Iab	M1 I	Per OB1-D	
HD 14580	02 23 24.11	+57 12 43.0	8.45	2.27	5.43	2	M0 Iab	M1 I	Per OB1-D	
HD 14826	02 25 21.86	+57 26 14.1	8.24	2.32	6.28	2	M2 Iab	M2 I	Per OB1-D	
HD 236979	02 38 25.42	+57 02 46.1	8.20	2.35	6.17	4	M2 Iab	M2 I	Per OB1-D?	YZ Per
W Per	02 50 37.89	+56 59 00.3	10.39	2.53	8.30	4	M3 Iab	M4.5 I	Per OB1-D?	HD 237008
BD +57°647	02 51 03.95	+57 51 19.9	9.52	2.74	. . .	4	M2 Iab	M2 I	Per OB1-D?	HD 237010
HD 17958	02 56 24.65	+64 19 56.8	6.24	2.03	. . .	1	K3 Ib	K2 I	Cam OB1	
HD 23475[e]	03 49 31.28	+65 31 33.5	4.48	1.88	. . .	5	M2+ IIab	M2.5 II	. . .	
HD 33299	05 10 34.98	+30 47 51.1	6.72	1.62	. . .	6	K1 Ib	K1 I	Aur OB1	
HD 35601	05 27 10.22	+29 55 15.8	7.35	2.20	5.61	2	M1 Ib	M1.5 I	Aur OB1	
HD 36389[e]	05 32 12.75	+18 35 39.2	4.38	2.07	. . .	1	M2 Iab–Ib	M2 I	. . .	
HD 37536[f]	05 40 42.05	+31 55 14.2	6.21	2.09	5.28	3	M2 Iab	M2 I	Aur OB1	
α Ori[e]	05 55 10.31	+07 24 25.4	0.50	1.85	. . .	1	M1–M2 Ia–Ib	M2 I	. . .	
HD 42475[e]	06 11 51.41	+21 52 05.6	6.56	2.25	5.70	3	M0–M1 Iab	M1 I	Gem OB1	TV Gem
HD 42543[e]	06 12 19.10	+22 54 30.6	6.39	2.24	5.46	3	M1–M2 Ia–Iab	M0 I	Gem OB1	BU Gem
HD 44537[e]	06 24 53.90	+49 17 16.4	4.91	1.97	. . .	1	K5–M0 Iab–Ib	M0 I	. . .	
HD 50877[e]	06 54 07.95	−24 11 03.2	3.86	1.74	. . .	6	K2.5 Iab	K2.5 I	Coll 121	o^1 CMa
HD 52005[e]	07 00 15.82	+16 04 44.3	5.68	1.63	. . .	3	K3 Ib	K5 I	. . .	
HD 52877[e]	07 01 43.15	−27 56 05.4	3.41	1.69	3.90	6	K7 Ib	M1.5 I	Coll 121	σ CMa
CD −31°4916	07 41 02.63	−31 40 59.1	8.91	2.16	5.20	1	M2 Iab	M2.5 I	NGC 2439	
HD 63302[e]	07 47 38.53	−15 59 26.5	6.35	1.78	. . .	5	K1 Ia–Iab	K2 I	. . .	
HD 90382	10 24 25.36	−60 11 29.0	7.45	2.21	6.05	4	M3 Iab	M3–M4 I	Car OB1-D	CK Car
HD 91093	10 29 35.37	−57 57 59.0	8.31	2.21	6.65	4	M2 Iab	M2 I	Car OB1-A	
CPD −57°3502[e]	10 35 43.71	−58 14 42.3	7.44	2.02	5.17	4	M1.5 Iab–Ib	M1.5 I	Car OB1-B/NGC 329	
HD 303250	10 44 20.04	−58 03 53.5	8.92	2.51	. . .	4	M3 Iab	M2 I	Car OB1-B?	
CD −58°3538[e]	10 44 47.15	−59 24 48.1	8.36	2.31	6.54	4	M2+ Ia–0	M2 I	Car OB1-E	RT Car
HD 93420[e]	10 45 50.63	−59 29 19.5	7.55	1.87	6.15	4	M4 Ib	M4 I	Car OB1-E	BO Car
HD 94096	10 50 26.30	−59 58 56.5	7.38	2.24	5.64	4	M2 Iab	M2 I	Car OB1-E	IX Car
HD 95687	11 01 35.76	−61 02 55.8	7.35	2.12	5.81	4	M2 Iab	M3 I	Car OB2	
HD 95950	11 03 06.15	−60 54 38.6	6.75	2.04	5.18	4	M2 Ib	M2 I	Car OB2	
HD 97671	11 13 29.97	−60 05 28.8	8.39	2.52	7.42	4	M3 Ia	M3–M4 I	Car OB2[g]	
CD −60°3621	11 35 44.96	−61 34 41.0	7.27	1.92	4.74	4	M0 Ib	M1.5 I	NGC 3766	
HD 100930[e]	11 36 26.22	−61 19 10.0	7.78	1.95	5.68	4	M2.5 Iab–Ib	M2.5 I	. . .	
CD −60°3636	11 36 34.84	−61 36 35.1	7.62	1.81	. . .	4	M0 Ib	M0 I	NGC 3766	
V396 Cen	13 17 25.05	−61 35 02.3	7.85	2.15	6.74	4	M4 Ia–Iab	M3–M4 I	Cen OB1-D	HD 115283
CPD −53°7344	16 12 56.91	−54 13 13.8	8.79	1.78	. . .	4	K2 Ib	K2 I	NGC 6067	
CPD−53 7364	16 13 04.01[d]	−54 12 21.2[d]	9.13	1.86	. . .	4	K4 Ib	K2 I	NGC 6067	
HD 160371[e]	17 40 58.55	−32 12 52.1	6.14	1.82	. . .	1	K2.5 Ib	K2.5 I	M6	BM Sco
α Her[e]	17 14 38.86	+14 23 25.2	3.06	1.45	. . .	3	M5 Ib–II	M5 I	. . .	
KW Sgr	17 52 00.73	−28 01 20.5	9.35	2.78	7.98	4	M3 Ia	M1.5 I	Sgr OB5	HD 316496
HD 175588[e]	18 54 30.28	+36 53 55.0	4.30	1.67	. . .	5	M4 II	M4 II	. . .	δ^2 Lyr
HD 181475[e]	19 20 48.31	−04 30 09.0	6.96	2.14	. . .	6	M0 II	M1 II	. . .	
HD 339034	19 50 11.93	+24 55 24.2	9.36	3.05	. . .	1	M1 Ia	K3 I	Vul OB1	Case 15
BD +35°4077	20 21 12.37	+35 37 09.8	9.72	2.93	8.11	3	M3 Iab	M2.5 I	Cyg OB1	
BD +36°4025	20 21 21.88	+36 55 55.7	9.33	2.49	8.75	3	M3 Ia	M3–M4 I	Cyg OB1	BI Cyg
BD +37°3903	20 21 38.55	+37 31 58.9	9.97	3.26	9.75	3	M3.5 Ia	M3 I	Cyg OB1	BC Cyg
KY Cyg	20 25 58.08[d]	+38 21 07.0[d]	10.57	3.64	10.40	4	M3 Ia	M3–M4 I	Cyg OB1	Case 66
BD +39°4208[e]	20 28 50.59	+39 58 54.4	8.69	2.87	8.21	1	M3–M4 Ia–Iab	M3 I	Cyg OB9	RW Cyg
HD 200905[e]	21 04 55.86	+43 55 40.2	3.70	1.65	. . .	5	K4.5 Ib–II	K4.5 I	. . .	
HD 202380[e]	21 12 47.25	+60 05 52.8	6.62	2.39	. . .	2	M2– Ib	M2 I	Cep OB2-A	
HR 8248	21 33 17.89	+45 51 14.4	6.23	1.78	. . .	7	K4 Ib	K1 I	Cyg OB7	HD 205349

TABLE 1—*Continued*

Star	α_{2000}	δ_{2000}	Photometry V	$B-V$	$V-K$	Ref.[b]	Spectral Type Old[c]	New	OB Association[a]	Comment
HD 206936[e]	21 43 30.46	+58 46 48.1	4.08	2.35	5.96	1	M2 Ia	M1 I	Cep OB2-A	μ Cep
HD 210745[e]	22 10 51.28	+58 12 04.5	3.35	1.55	...	5	K1.5 Ib	K1.5 I	...	
BD +56°2793	22 30 10.73	+57 00 03.1	8.09	2.28	6.22	3	M2 Ia	M3 I	Cep OB2-B	HD 239978, ST Cep
Case 75	22 33 34.64[d]	+58 53 47.1[d]	10.67	3.18	...	4	M1 Ia	M2.5 I	Cep OB1[g]	V354 Cep[h]
Case 78	22 49 10.46[d]	+59 18 12.9[d]	10.76	2.30	...	4	M2 Ib	M2 I	Cep OB1[g]	V355 Cep[h]
HD 216946[e]	22 56 26.00	+49 44 00.8	4.94	1.77	...	5	M0– Ib	M0 I	Lac OB1[h]	
Case 80	23 10 10.90	+61 14 29.9	9.72	2.60	...	4	M2 Iab	M3 I	Cas OB2	GU Cep
Case 81	23 13 31.50[d]	+60 30 18.5[d]	9.92	2.70	...	4	M2 Ia	M2 I	Cas OB2	V356 Cep?
HD 219978	23 19 23.77	+62 44 23.2	6.77	2.27	...	2	K5 Ib	M1 I	Cep OB3	V809 Cas
BD +60°2613	23 44 03.28	+61 47 22.2	8.50	2.77	7.48	1	M4 Ia	M3 I	Cas OB5	PZ Cas
BD +60°2634	23 52 56.24	+61 00 08.3	9.17	2.51	7.22	3	M2 Iab	M3 I	Cas OB5	TZ Cas

Note.—Units of right ascension are hours, minutes, and seconds, and units of declination are degrees, arcminutes, and arcseconds.
[a] OB association membership from Humphreys (1978) and Garmany & Stencel (1992). For Per OB1 and Car OB1, the subgroups identified by Mel'Nik & Efremov (1995) have been used, based on the star's l and b.
[b] The K data come from Josselin et al. (2000) and references therein.
[c] Old spectral types are from Humphreys (1978) and references therein, except for the standard stars, for which the types are from Morgan & Keenan (1973).
[d] Coordinates new to this study. In some cases these are based on 2MASS positions.
[e] Spectral standard from Morgan & Keenan (1973).
[f] Possible AGB; see Josselin et al. (2003).
[g] Membership listed as questionable by Humphreys (1978), but see also Garmany & Stencel (1992).
[h] Incorrectly cross-referenced to the BD catalog by Garmany & Stencel (1992).
References.—(1) Nicolet 1978; (2) Humphreys 1970; (3) Lee 1970; (4) Humphreys 1978 and references therein; (5) Johnson et al. 1966; (6) Fernie 1983; (7) Jennens & Helfer 1975.

flexure. Observations of spectrophotometric standards were obtained throughout the night.

We reduced the data using Image Reduction and Analysis Facility (IRAF)[5] packages `ccdred`, `kpnoslit`, and `ctioslit`. We used dome flats to flatten the blue Kitt Peak data and the projector lamps to flatten the red Kitt Peak data. We found that the only shift in the fringe pattern in the red occurred during the 30 minutes following a refill of the dewar with liquid nitrogen. After that the fringe pattern was stable, so we simply combined these projector flats. The spectra were all extracted using an optimal extraction algorithm. When reducing the CTIO data the narrow slit width observations were combined and divided into the wide-slit observations. The resulting division was fit with a low-order function and used to correct the fluxes of the narrow-slit observations. In a few cases the wide-slit observations included the presence of an additional star in the extraction aperture; these stars were eliminated from further consideration and do not appear in Table 1.

The observations of spectrophotometric standards were used to create sensitivity functions; typically a gray shift was applied to each night's data, and the resulting scatter was 0.02 mag. In addition, the different wavelength regions were grayshifted to agree in the regions of overlap.

When we began our analysis we found significant discrepancies between the reddened model atmospheres and the observed spectra in the near-ultraviolet (near-UV) region (<4000 Å for the reddest stars). Careful investigations suggest that, despite the excellent agreement of the spectrophotometric standards, there could be contamination by a grating ghost in the near-UV, in which a small fraction of the red light contaminates the data. The expected flux ratio $F_{\lambda 7000}/F_{\lambda 3500}$ is roughly 10,000 for the most reddened M supergiants, a regime seldom encountered in astronomical spectrophotometry. We do not know if this contamination is a small fraction of the near-UV light or if it dominates, and we have therefore restricted our study to the data longward of 4100 Å, where our tests show that the ghosting effect is negligible. We revisit this issue in Massey et al. (2005).

[5] IRAF is distributed by NOAO, which is operated by AURA, Inc., under cooperative agreement with the NSF.

3. ANALYSIS

3.1. *Reclassification of Spectral Type*

We reclassified each of our stars by visually comparing each spectrum to the spectral standards. In order to avoid questions of normalizing these rich and complicated spectra (with uncertain continuum levels), we did this comparison in terms of log flux. Given that many of these stars can be variable in spectral type, we were unsurprised to find that we needed to reclassify a few of the spectral standards for consistency. For the late-K and all M-type stars, the classification was based on the depths of the TiO bands, which are increasingly strong with later spectral type. The reclassification of the early and mid-K supergiants was based primarily on the strengths of the G band plus the strength of Ca I λ4226. These features all get weaker with later spectral types (Jaschek & Jaschek 1987), a temperature effect that we confirmed with the MARCS models. We list our revised spectral types in Table 4.

3.2. *Modeling the Stars: Effective Temperatures and Reddenings*

We compared the observed spectral energy distribution (SED) of each star to a series of MARCS stellar atmosphere models. The models used in our comparisons ranged from 3000 to 4300 K in increments of 100 K, with log g from +1.0 to −1.0 in increments of 0.5 dex. The choice of surface gravity was derived iteratively; we began by adopting the log $g = -0.5$ models for all of the fits, as this surface gravity was generally what was expected with the old effective temperature scale and the resulting placement in the H-R diagram. However, our new temperatures were a bit warmer than those predicted by the old scale, so we reevaluated all of the fits using log $g = 0.0$, as this was more consistent with the revised

TABLE 2

Adopted Distance Moduli and Average Reddenings

OB Assoc./Cluster[a]	l (deg)	b (deg)	$(m-M)_0$ (mag) Value	Ref.	Value	Ref.	Adopted	$E(B-V)_{\rm cluster}$[b] (mag)	Additional $(m-M)_0$, (Ref.)
Cas OB4	119.5	−0.4	11.0	1	12.3	2	11.6	0.70 ± 0.21	
Cas OB7	123.5	0.9	12.0	2	...	...	12.0	0.83 ± 0.14	
NGC 457	126.6	−4.4	12.0	2	11.9	3	11.9	0.51 ± 0.04	
Cas OB8/NGC 581	128.0	−1.8	11.9	4	11.7	3	11.8	0.38	
Cas OB8/NGC 663	129.5	−1.0	11.6	4	11.5	3	11.5	0.78	
Cas OB8	129.4	−0.9	11.2	1	12.3	2	11.7	0.69 ± 0.19	
Per OB1-A	131.1	−1.5	11.0	1	11.8	2	11.4	0.66 ± 0.19	
Per OB1-D	135.0	−3.5	11.4	1	11.8	2	11.4	0.66 ± 0.19	
Per OB1-D/NGC 884	135.1	−3.6	12.0	4	11.9	3	11.9	0.56	
Cam OB1	140.4	1.9	10.0	1	10.0	2	10.0	0.74 ± 0.21	
Aur OB1	174.6	1.2	10.7	1	10.6	2	10.7	0.47 ± 0.15	
Gem OB1	188.9	3.4	10.6	1	10.9	2	10.7	0.66 ± 0.24	
Coll 121	237.9	−7.7	8.9	5	8.4	3	8.4	0.03	
NGC 2439	246.4	−4.4	13.2	2	12.9	3	13.0	0.57 ± 0.24	
Car OB1-A	284.5	−0.0	11.9	1	12.0	2	11.9	0.48 ± 0.11	
Car OB1-B/NGC 3293	285.9	+0.1	12.0	2	11.8	3	11.9	0.30	
Car OB1-B	286.0	0.5	11.7	1	12.0	2	11.9	0.55 ± 0.21	
Car OB1-D	286.6	−1.8	11.9	1	12.0	2	11.7	0.55 ± 0.21	
Car OB1-E	287.6	−0.7	12.1	1	12.0	2	12.0	0.55 ± 0.21	
Car OB2	290.6	−0.1	11.7	1	11.5	2	11.6	0.48 ± 0.18	
NGC 3766	294.1	−0.0	11.6	1	11.7	6	11.6	0.20 ± 0.10	11.2 (3)
Cen OB1-D	305.5	1.6	11.4	1	12.0	2	11.6	0.75 ± 0.25	
NGC 6067	329.8	−2.2	11.6	2	10.8	3	10.8	0.32 ± 0.07	
M 6	356.6	−0.7	8.3:	2	8.4	3	8.4	0.14	
Sgr OB5	0.2	−1.3	12.4	2	...	...	12.4	0.92 ± 0.33	
Vul OB1	59.4	−0.1	12.0	1	11.5	2	11.8	0.94 ± 0.20	12.7 (7)
Cyg OB1	75.6	1.1	10.7	1	11.3	2	11.0	0.93 ± 0.33	
Cyg OB9	76.8	1.4	10.7	1	10.4	2	10.6	1.22 ± 0.32	
Cep OB2-A	99.3	3.8	9.9	1	9.6	2	9.7	0.66 ± 0.19	9.0 (5)
Cep OB2-B	103.6	5.6	9.4	1	9.6	2	9.5	0.66 ± 0.19	9.0 (5)
Cep OB1	108.5	−2.7	11.7	1	12.7	2	12.2	0.63 ± 0.17	
Cyg OB7	90.0	2.0	9.5	2	9.6	8	9.5	0.65 ± 0.40	
Lac OB1	96.8	16.1	9.0	1	8.9	9	8.9	0.11:	7.8 (5)
Cas OB2	112.0	0.0	12.1	2	...	...	12.1	0.99 ± 0.25	
Cep OB3	110.4	2.9	9.6	1	9.7	2	9.7	0.84 ± 0.10	
Cas OB5	115.5	0.3	11.8	1	12.0	2	11.9	0.69 ± 0.14	

[a] Either classical names, or in the case of the subdivided associations taken from Mel'Nik & Efremov (1995).

[b] Average $E(B-V)$ computed from Humphreys (1978), using only the early-type stars and excluding any stars whose spectroscopic parallaxes differ from the mean by more than 1 mag. The uncertainties listed are the 1 σ range of these values, giving an indication of how variable the extinction is over the face of the region.

References.—(1) Mel'Nik & Efremov 1995; (2) Humphreys 1978; (3) WEBDA (Mermilliod & Paunzen 2003); (4) Becker & Fenkart 1971; (5) de Zeeuw et al. 1999; (6) Moitinho et al. 1997; (7) Sagar & Joshi 1981; (8) Bochkarev & Sitnik 1985; (9) Ruprecht 1966.

TABLE 3

Observation Parameters

Parameter	KPNO 2.1 m Blue	KPNO 2.1 m Red	CTIO 1.5 m Blue	CTIO 1.5 m Orange	CTIO 1.5 m Red
Grating/line mm^{-1}	26/600	58/400	26/600	58/400	58/400
Blocking Filter	none	GG495	none	GG495	OG570
Wavelength Coverage (Å)	3200[a]–6000	5000–9000	3500[a]–5200	5000–7500	6300–9000
Slit Width (arcsec/μm)	3.0/250	2.1/170	4.9/270	3.6/200	3.6/200
Dispersion (Å mm^{-1})	1.3	1.9	1.5	2.2	2.2
Resolution (Å)	3.6	5.7	5.0	6.4	6.4

[a] Spectrophotometry below ~4100 Å may be contaminated by a grating problem for the reddest stars and is not discussed further.

TABLE 4

RESULTS OF MODEL FITS

STAR	SPECTRAL TYPE	T_{eff}	A_V	log g[a] Model	log g[a] Actual[d]	$R/R_\odot$[a,b]	M_V[b]	M_{bol}[a,b]	ΔA_V[c]
BD +59°38	M2 I	3650	3.10	0.0	0.1	600	−5.57	−7.17	0.92
Case 23	M3 I	3600	3.25	0.5	0.3	410	−4.53	−6.28	0.69
HD 236697	M1.5 I	3700	1.55	0.5	0.4	380	−4.80	−6.25	−0.04
BD +59°274	M1 I	3750	1.55	0.5	0.4	360	−4.80	−6.14	0.37
BD +60°335	M4 I	3525	2.63	0.0	0.1	610	−4.99	−7.05	0.22
HD 236871	M2 I	3625	2.17	0.0	0.2	520	−5.13	−6.80	0.03
HD 236915	M2 I	3650	1.71	0.0	0.3	420	−4.80	−6.40	−0.33
BD +59°372	K5–M0 I	3825	2.48	0.5	0.6	290	−4.58	−5.77	0.45
BD +56°512	M3 I	3600	3.25	0.5	0.1	620	−5.42	−7.17	1.22
HD 14469	M3–4 I	3575	2.01	0.0	−0.1	780	−5.78	−7.64	−0.02
HD 14488	M4 I	3550	2.63	0.0	−0.3	1000	−6.18	−8.15	0.90
HD 14528	M4.5 I	3500	4.18	−0.5	−0.4/−0.1	1230/780	−6.36	−8.53/−7.53	2.15
BD +56°595	M1 I	3800	1.86	0.0	0.4	380	−5.08	−6.31	−0.17
HD 14580	M1 I	3800	2.17	0.5	0.4	380	−5.12	−6.35	0.14
HD 14826	M2 I	3625	2.48	0.0	0.0	650	−5.64	−7.31	0.45
HD 236979	M2 I	3700	2.32	0.0	0.2	540	−5.52	−6.97	0.29
W Per	M4.5 I	3550	4.03	0.0	0.1	620	−5.13	−7.09	2.00
BD +57°647	M2 I	3650	4.03	0.0	0.0	710	−5.91	−7.51	2.00
HD 17958	K2 I	4200	2.17	0.5	0.5	360	−5.93	−6.63	−0.12
HD 23475	M2.5 II	3625	1.08	0.0	...	...	...	...	...
HD 33299	K1 I	4300	0.77	0.5	0.9	190	−4.76	−5.37	−0.69
HD 35601	M1.5 I	3700	2.01	0.0	0.2	500	−5.36	−6.81	0.55
HD 36389	M2 I	3650	1.24	0.0	...	...	...	...	...
HD 37536	M2 I	3700	1.39	0.0	0.1	630	−5.88	−7.33	−0.07
α Ori	M2 I	3650	0.62	0.0	...	...	...	...	...
HD 42475	M1 I	3700	2.17	0.0	−0.1	770	−6.31	−7.76	0.13
HD 42543	M0 I	3800	2.01	0.0	0.0	670	−6.32	−7.55	−0.03
HD 44537	M0 I	3750	0.62	0.0	...	...	...	...	...
HD 50877	K2.5 I	3900	0.16	0.5	0.6	280	−4.69	−5.75	0.06
HD 52005	K5 I	3900	0.00	0.0	...	...	...	...	...
HD 52877	M1.5 I	3750	0.16	0.5	0.3	420	−5.14	−6.48	0.06
CD −31°4916	M2.5 I	3600	2.01	0.0	−0.1/0.2	850/500	−6.11	−7.85/−6.69	0.23
HD 63302	K2 I	4100	0.62	0.0	...	...	...	...	...
HD 90382	M3–M4 I	3550	1.86	0.0	−0.3	1060	−6.31	−8.27	0.16
HD 91093	M2 I	3625	2.01	0.0	0.0	640	−5.60	−7.28	0.50
CPD −57°3502	M1.5 I	3700	1.08	0.0	0.2	540	−5.54	−6.99	0.15
HD 303250	M2 I	3625	2.94	0.0	−0.1	750	−5.92	−7.60	1.24
CD −58°3538	M2 I	3625	3.10	0.0	−0.3	1090	−6.74	−8.41	1.40
HD 93420	M4 I	3525	1.08	0.0	−0.1	790	−5.53	−7.60	−0.62
HD 94096	M2 I	3650	1.86	0.0	−0.2	920	−6.48	−8.08	0.16
HD 95687	M3 I	3625	1.71	0.0	−0.1	760	−5.96	−7.63	0.21
HD 95950	M2 I	3700	1.24	0.0	0.0	700	−6.09	−7.54	−0.25
HD 97671	M3–M4 I	3550	2.63	0.0	−0.2	860	−5.85	−7.81	1.14
CD −60°3621	M1.5 I	3700	0.77	0.0	0.3	440	−5.11	−6.55	0.15
HD 100930	M2.5 I	3600	1.08	0.0	...	...	...	...	...
CD −60°3636	M0 I	3800	0.77	0.5	0.5	320	−4.76	−5.98	0.15
V396 Cen	M3–M4 I	3550	2.48	0.0	−0.3	1070	−6.33	−8.29	0.16
CPD −53°7344	K2 I	4000	0.77	1.0	1.3	100	−2.78	−3.70	−0.21
CPD −53°7364	K2 I	4000	1.08	1.0	1.3	100	−2.76	−3.67	0.10
HD 160371	K2.5 I	3900	0.31	1.0	1.3	100	−2.57	−3.63	−0.12
α Her[e]	M5 I	3450	1.40	0.0	...	...	...	...	...
KW Sgr	M1.5 I	3700	4.65	−0.5	−0.5	1460	−7.70	−9.15	1.81
HD 175588	M4 II	3550	0.47	0.0	...	...	...	...	...
HD 181475	M1 II	3700	1.39	0.0	...	...	...	...	...
HD 339034	K3 I	4000	5.27	0.0	−0.2	980	−7.71	−8.63	2.34
BD +35°4077	M2.5 I	3600	5.27	0.0	−0.3/0.1	1040/620	−6.55	−8.30/−7.18	2.39
BD +36°4025	M3–M4 I	3575	5.11	−0.5	−0.4	1240	−6.78	−8.64	2.23
BD +37°3903	M3 I	3575	5.58	−0.5	−0.3	1140	−6.61	−8.46	2.70
KY Cyg	M3–M4 I	3500	7.75	−1.0	−0.9/−0.5	2850/1420	−8.18	−10.36/−8.84	4.87
BD +39°4208	M3 I	3600	4.49	0.0	−0.2	980	−6.41	−8.15	0.69
HD 200905	K4.5 I	3800	0.00[f]	0.0[f]	...	...	...	...	...
HD 202380	M2 I	3700	2.63	0.0	0.1	590	−5.72	−7.16	0.59
HR 8248	K1 I	4000	0.93	1.0	0.9	200	−4.20	−5.12	−0.82

TABLE 4—*Continued*

Star	Spectral Type	$T_{\rm eff}$	A_V	log g[a] Model	log g[a] Actual[d]	$R/R_\odot$[a,b]	M_V[b]	$M_{\rm bol}$[a,b]	ΔA_V[c]
HD 206936	M1 I	3700	2.01	−0.5	−0.5	1420	−7.63	−9.08	−0.03
HD 210745	K1.5 I	4000	0.00	0.0	...	...	...	...	...
BD +56°2793	M3 I	3600	2.32	0.5	0.6	290	−3.73	−5.48	0.28
Case 75	M2.5 I	3650	6.05	−0.5	−0.5	1520	−7.57	−9.17	4.10
Case 78	M2 I	3650	4.65	0.0	−0.1	770	−6.09	−7.69	2.71
HD 216946	M0 I	3800	0.31	0.5	0.7	260	−4.27	−5.50	−0.02
Case 80	M3 I	3625	2.94	0.0	0.1	570	−5.32	−7.00	−0.12
Case 81	M2 I	3700	3.56	0.0	0.1	590	−5.74	−7.19	0.50
HD 219978	M1 I	3750	2.17	0.5	0.4	410	−5.10	−6.44	−0.42
BD +60°2613	M3 I	3600	4.49	−0.5	−0.7/−0.4	1940/1190	−7.89	−9.64/8.57	2.38
BD +60°2634	M3 I	3600	3.25	0.0	−0.1	800	−5.98	−7.73	1.13

[a] In the case of the five stars whose $M_{\rm bol}$ found from K differ significantly from that found from V, we list both values, with the V-values first.
[b] Given the 0.1 mag estimated error in $E(B-V)$, we expect that the M_V and $M_{\rm bol}$ values are determined to approximately 0.3 mag. Add to this the 50–100 K uncertainty in $T_{\rm eff}$, and the uncertainty in $R/R_\odot$ is roughly 20%.
[c] $\Delta A_V = A_V({\rm RSG}) - 3.1E(B-V)_{\rm cluster}$.
[d] Based on adopting an approximate mass $\log(M/M_0) = 0.50 - 0.10M_{\rm bol}$.
[e] The fit for α Her is poor in the blue, as shown in the online figure, due presumably to the very close (0.″2) companion known from interferometry. The star is listed as WDS 17146+1426 in Mason et al. (2001).
[f] The low reddening likely suggests a slightly higher surface gravity would be appropriate for this standard.

locations in the H-R diagram. The effective temperatures remained unchanged with the use of these higher surface gravities (except for the occasional star), but the values of $E(B-V)$ increased slightly. Finally, we used the revised temperature scale and bolometric luminosities with the evolutionary tracks (§ 3.3) to compute log g star by star for the RSGs with distances. This confirmed that our choice of the log $g = 0.0$ models was appropriate for most of the stars. We refit the stars using the appropriate log g if the distance was known; otherwise, we adopted log $g = 0.0$. In practice the choice of log g affected the derived values of $E(B-V)$ by <0.1 mag and had no effect on the derived effective temperatures.

In making the fits, we reddened each model using a Cardelli et al. (1989) reddening law with the standard ratio of total-to-selective extinction $R_V = 3.1$.[6] Our initial guess for $E(B-V)$ was based on the average value for the cluster, i.e., $E(B-V)_{\rm cluster}$ from Table 2. The temperature was determined primarily from the strengths of the TiO bands (M supergiants) and the G band (early to mid-K supergiants), with $E(B-V)$ then adjusted to produce the best fit to the continuum. In Figure 1 we show a sample of spectra and fits, covering a range of spectral types; the complete set is available in the electronic edition of the Journal. The fitting was all done in log units of flux in order to facilitate comparisons of line intensities without the uncertain process of normalization, as mentioned previously.

As described in § 2, our initial modeling revealed a significant discrepancy between the models and the data in the near-UV region (3500–4000 Å) for the reddest stars, which we first attributed to a peculiar reddening law caused, we argued, by circumstellar dust. However, since we cannot exclude the possibility that the near-UV data are affected by an instrumental problem, we will revisit this issue at a later time when we have better data in the near-UV. See Massey et al. (2005).

Otherwise, the agreement between the SEDs of the reddened models and the data is extremely good, both in terms of the continua and molecular band depths. The only significant problem we encountered was for the early to mid-K stars, where we expected to use both the Ca I λ4226 line, as well as the G band in modeling the stars, as these lines are among the primary classification lines for the early K stars. However, we found that these Ca I lines were stronger in the MARCS models' synthetic spectra than in our stars, usually by a factor of 3 or so. The Ca I line shows the same qualitative behavior with effective temperature as expected (see above discussion), but the absolute line strengths in the models were too strong. Since Ca has a very low ionization potential (6.11 eV), most of the Ca is in the form of Ca II: ~99% in the model at 4000 K and 98% in the model at 3600 K (at an optical depth of 0.01 for the continuum). Thus, a small overionization will strongly impact the line strength, due to either the effects of non-LTE or a slight error in the model's temperature structure. The occurrence of cool or hot spots on the stellar surface could also lead to regions where the ionization equilibrium is strongly affected.

In addition to the problem with the Ca I line, the models also produce Ca II H and K lines that are significantly stronger than those observed, even in those stars for which the fluxes of the dereddened stars and the stars were in good agreement. This is not hard to understand, as RSGs are expected to have chromospheric activity, and this is not accounted for in the models. The presence of a chromosphere would lead to emission in the H and K lines, resulting in weaker observed lines than would be the case if the lines were purely photospheric in origin. This explanation could be further investigated by means of high-dispersion spectroscopy.

We relied instead on the G band for the fitting of the early and mid-K stars. We substantiated that we obtained similar temperatures using the G band and the TiO bands for the late K stars. The resulting temperature fits for the early and mid-K stars are therefore less certain, probably ±100 K.

[6] The value R_V is typically taken to be ~3.6 for RSGs (Lee 1970), due to the increase of the effective wavelength of broadband filters with redder stars; see McCall (2004) for a recent discussion. Our own calculations from the models suggest that $R_V \sim 4.4$ would be more appropriate for BV photometry of RSGs. Note, however, that in the absence of a peculiar reddening law, $R_V = 3.1$ is an appropriate choice for our study, since our analysis is not based on broadband filter photometry but rather on moderate-resolution (5 Å) SEDs; i.e., neither the B nor V filters were involved in our extinction determinations. In order to prevent confusion, we use the equivalent A_V values rather than $E(B-V)$, as our A_V values will be directly comparable to those of others, while our $E(B-V)$ values would be larger than those determined from broadband photometry for RSGs.

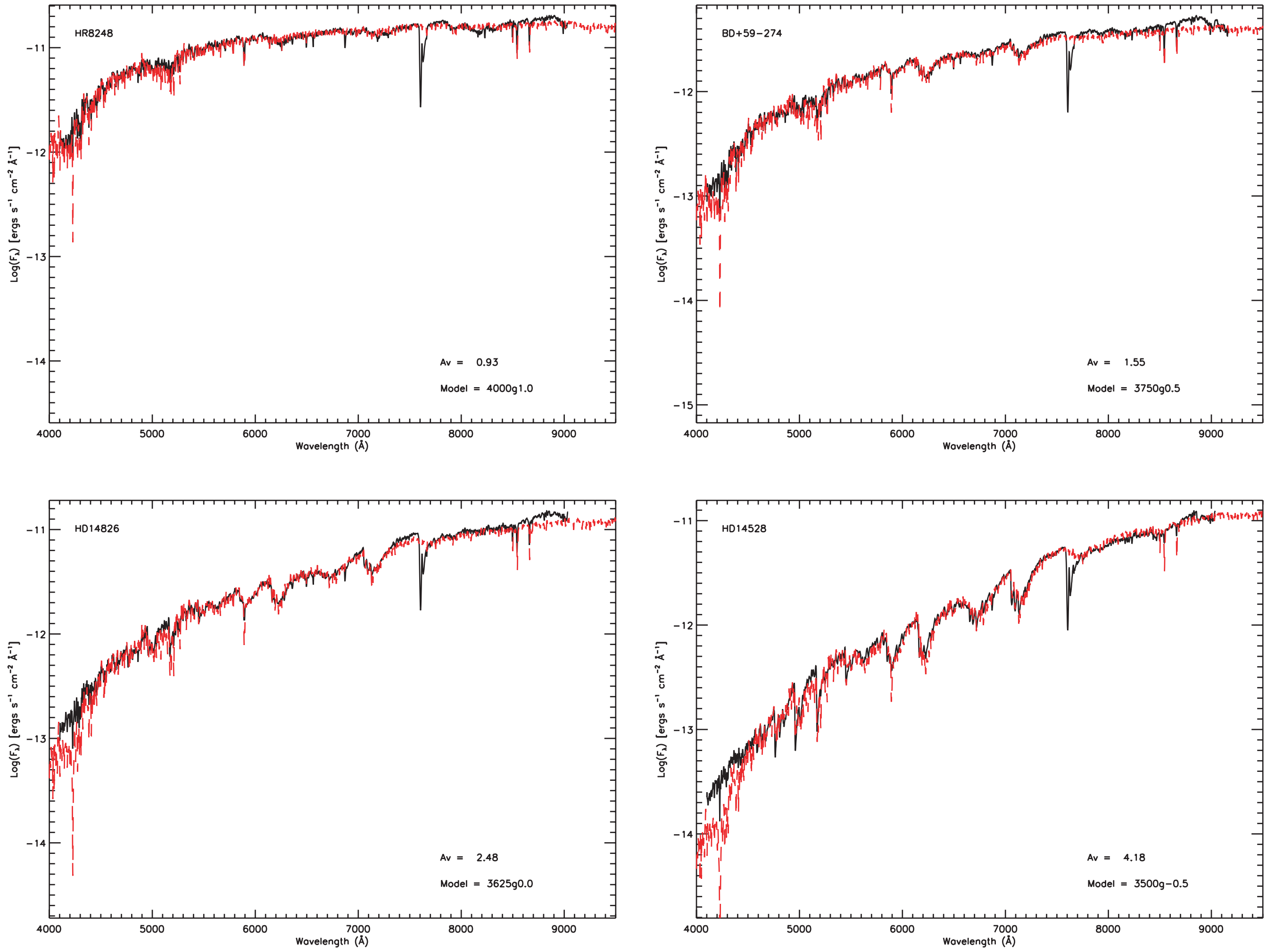

Fig. Set 1.—Spectrophotometry (*solid black line*) and the MARCS model comparisons (*dotted red line*). The data are plotted on a log F_λ scale to facilitate comparison between the size of the molecular transitions. The models have been reddened by the indicated amount using the standard $R_V = 3.1$ reddening law of Cardelli et al. (1989). The four sample stars shown here have spectral types K1 I (HR 8248), M1 I (BD +59°274), M2 I (HD 14826), and M4.5 I (HD 14528). [*See the electronic version of the Journal for Figs. 1.1–1.78.*]

We list the effective temperatures in Table 4. In general, we found that the data could be matched very well by the models, *both* in line strength and in continuum shape, and we expect that the effective temperatures of the M supergiants have been obtained to a precision of 50 K. The A_V values are determined to a precision of about 0.15 mag. We note with interest that the derived A_V values of about one third of our sample are significantly higher than the average found from the OB stars in the same associations and clusters using the data from Humphreys (1978); indeed, the same conclusion could have been drawn from the older data given in that paper. A possible interpretation is that this extra extinction is due to circumstellar dust. We include the ΔA_V values in Table 4. We will revisit this issue in a subsequent paper, once our analysis of the Magellanic Cloud data (where the foreground reddening is low and relatively uniform) is complete.

Our new effective temperature scale is given in Table 5, where we include the number of stars and standard deviation of the mean (σ_μ) at each spectral type. We compare this scale to that of Humphreys & McElroy (1984) and Massey & Olsen (2003) in Figure 2. Both of the latter are "averages" from the literature. We see that the new scale agrees well for the K supergiants but is progressively warmer than past scales for later spectral types, with the differences amounting to 400 K by the latest M supergiants (M5 I). The overall progression of the temperature with later spectral type is more gradual than in past studies.

We include in Table 5 the BCs to the V band corresponding to the new effective temperature scale; these values are the linear interpolations of the BCs from the MARCS models given below.

TABLE 5

New Effective Temperature Scale RSGs

Spectral Type	$T_{\rm eff}$[a] (K)	σ_μ	N	BC
K1–K1.5	4100	100	3	−0.79
K2–K3	4015	40	7	−0.90
K5–M0	3840	30	3	−1.16
M0	3790	13	4	−1.25
M1	3745	17	7	−1.35
M1.5	3710	8	6	−1.43
M2	3660	7	17	−1.57
M2.5	3615	10	5	−1.70
M3	3605	4	9	−1.74
M3.5	3550	11	6	−1.96
M4–M4.5	3535	8	6	−2.03
M5	3450	. . .	1	−2.49

[a] Averages from Table 4, rounded to the nearest 5 K.

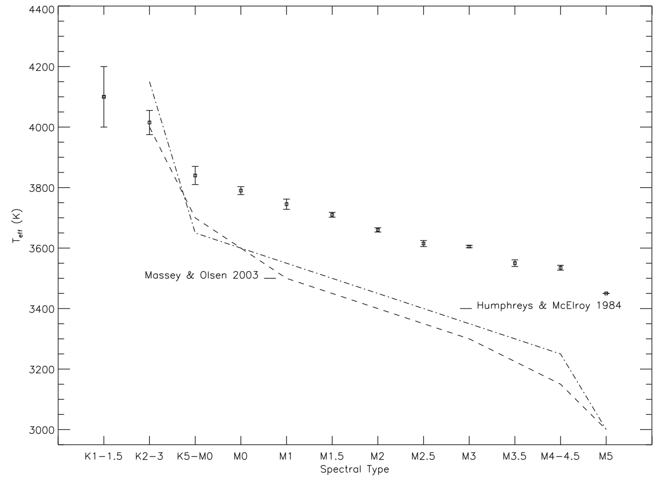

FIG. 2.—Effective temperature scale for Galactic RSGs. The error bars reflect the standard deviation of the means from Table 5. For comparison, we show the scales of Humphreys & McElroy (1984) and Massey & Olsen (2003).

The values are for $\log g = 0.0$, but there is little change with surface gravity (<0.05 mag over 0.5 dex in $\log g$ for 3500 K $\leq T_{\rm eff} \leq$ 4300 K). Note that we have referenced the BCs to the system advocated by Bessell et al. (1998), i.e., that the Sun has a BC of −0.07 mag. This results in values less luminous (by 0.12 mag) than the historical one; on this system the Sun is *defined* to have an $M_{\rm bol}$ of 4.74.

3.3. *Comparison to Evolutionary Models*

In order to compare these stars to the evolutionary models, we must convert the absolute visual luminosities to bolometric luminosities. In Table 6 we give the BCs as a function of effective temperature determined from the MARCS models. We list the bolometric magnitudes for each star with a known distance in Table 4.[7]

In Figure 3*a* we show the solar metallicity evolutionary tracks of Meynet & Maeder (2003) compared to the location of the

[7] We note that Josselin et al. (2003) have proposed that the star HD 37536 is an AGB based on the detection of Tc and Li. On the other hand, the star is seen projected against Aur OB1, and if membership is assumed, a sensible M_V is derived. In addition, the reddening is similar to that of the early-type members of Aur OB1.

TABLE 6
MARCS BCs[a]

$T_{\rm eff}$ (K)	BC_V	BC_K
3200	−4.58	3.16
3300	−3.66	3.08
3400	−2.81	3.00
3500	−2.18	2.92
3600	−1.75	2.84
3700	−1.45	2.76
3800	−1.23	2.68
3900	−1.06	2.61
4000	−0.92	2.53
4100	−0.79	2.47
4200	−0.70	2.40
4300	−0.61	2.33

[a] Computed for $\log g = 0.0$ models, with the zero point defined such that $BC_V = -0.07$ for the Sun; see Bessel et al. (1998).

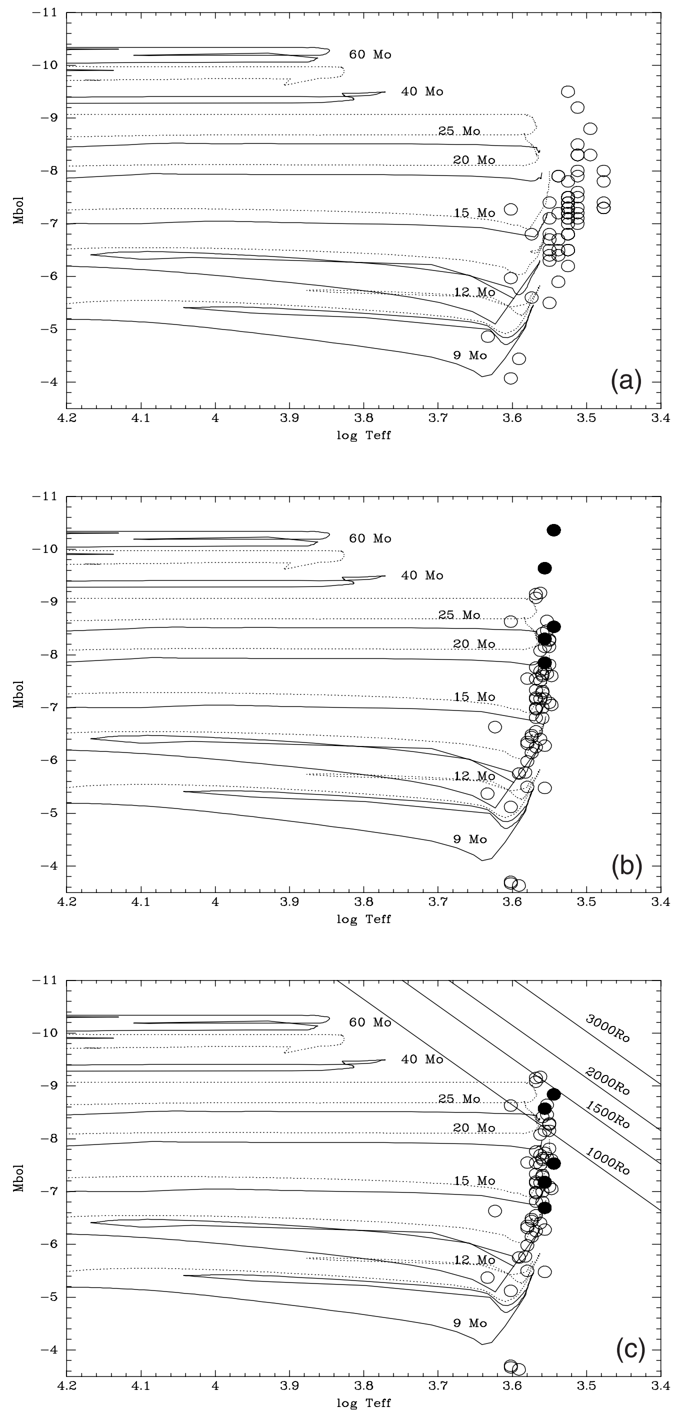

FIG. 3.—Comparison with evolutionary tracks. The evolutionary tracks of Meynet & Maeder (2003) are shown, along with the location of Galactic RSGs. The solid lines denote the no-rotation models, while the dotted lines show the evolutionary tracks for an initial rotation velocity of 300 km s^{-1}. The tracks with rotation appear above the no-rotation tracks; the one for 60 $M_\odot$ does not extend this far to the right in the H-R diagram. In (*a*) we show the location of the RSGs taken from Humphreys (1978), using the effective temperature and BCs of Humphreys & McElroy (1984). In (*b*) we show the location of the RSGs using our new model fits (from Table 4). The filled circles in (*b*) denote those five stars whose luminosities derived from *V* are significantly higher than those derived from *K*. In (*c*) we show these same five stars with the luminosities derived from *K*. The diagonal lines at upper right in this figure show lines of constant radii.

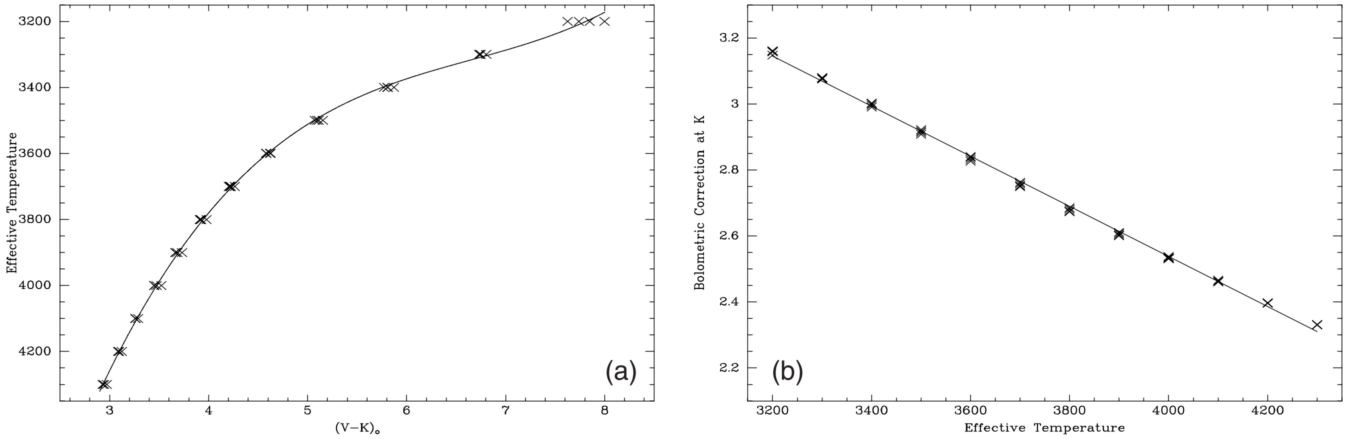

Fig. 4.—Derivation of (*a*) effective temperatures and (*b*) BCs at *K* based on the $(V-K)_0$ colors. The points were computed from the models, while the curve shows the smooth fits described in the text. The data extend from 3200 to 4300 K with log g values ranging from −1 to +1.

Galactic RSGs taken from Humphreys (1978) using the effective temperature and BCs of Humphreys & McElroy (1984). The disagreement is not as bad as that shown by Massey (2003), as the new tracks extend farther to the right at higher luminosities than did the older tracks of Schaller et al. (1992). Nevertheless, it is clear that there are significant differences between theory and "observation." In Figure 3*b* we now compare the same tracks to the Galactic RSGs using the new effective temperatures and bolometric models found by using the MARCS models. We have marked with filled symbols those five stars for which the *K*-band data suggest that our $M_{\rm bol}$ values are too luminous (§ 3.4), and in Figure 3*c* we show the location of these stars based on the *K*-band data. In Figures 3*b* and 3*c* the disagreement between theory and location in the H-R diagram has now disappeared, giving us some confidence in the accuracy of our new calibration. A few stars have luminosities significantly higher than the evolutionary tracks would predict (Fig. 3*b*), but these are invariably the stars whose $M_{\rm bol}$ values derived from *V* are at odds with those derived from *K* (Fig. 3*c*), presumably due to mistakes in the correction for reddening, and hence their value must be considered poorly determined; Figure 3*c* is the best determined.

The fact that we have both $M_{\rm bol}$ and $T_{\rm eff}$ allows us to determine the stellar radii $R/R_\odot$ from the formal definition of $T_{\rm eff}$; i.e., $(R/R_\odot) = (L/L_\odot)^{0.5}(T_{\rm eff}/5781\ {\rm K})^2$, where the numerical quantity is the effective temperature of the sun (see discussion in Bessell et al. 1998) and $L/L_\odot = 10^{-(M_{\rm bol}-4.74)/2.5}$. We include these values in Table 4. The stars with the largest radii in our sample, KW Sgr, Case 75, KY Cyg, and HD 206936 (=μ Cep),[8] all have radii of roughly 1500 $R_\odot$ (7 AU), making these the largest normal stars known. For comparison, Betelgeuse has a radius (measured by interferometry) of 645 $R_\odot$ (Perrin et al. 2004). We include in Figure 3*c* lines of constant radii. These four large stars are right at what current evolutionary theory predicts is the maximum radius for Galactic RSGs, as the largest radius reached by the tracks is found at roughly $M_{\rm bol} = -9$ and log $T_{\rm eff} = 3.57$ (3715 K).

Two peculiar RSGs are known with significantly larger radii. The M2 I primary in the interacting binary VV Cep has a radius that has been variously estimated as 1200 $R_\odot$ (Hutchings & Wright 1971) to 1600 $R_\odot$ (Wright 1977) and beyond, with a reasonable upper limit of 1900 $R_\odot$ determined by Saito et al. (1980); see discussion in Bauer & Bennett (2000). VV Cep consists of a RSG primary and a hotter companion orbiting within a common envelope. These estimates of the radii are complicated by the uncertainties in the orbital inclination in § 3 of Saito et al. (1980), with the "definition" of radius determined by the eclipse method leading to a further ambiguity. In any event, gravitational interactions are certainly taking place in this system (Hutchings & Wright 1971) and thus may not have applications to normal, single stars.

The other star with a humongous radius is VY CMa. Using interferometry with Keck, Monnier et al. (2004) find a photospheric radius of 14 AU (3020 $R_\odot$) for this star, where the distance of 1.5 kpc appears fairly certain from maser proper motions (Richards et al. 1998; see discussion in Monnier et al. 1999). The properties of this intriguing object have been recently discussed by Monnier et al. (1999) and Smith et al. (2001). With a luminosity of $2-5\times10^5\ L_\odot$ ($M_{\rm bol} = -8.5$ to -9.5) well established from the infrared (IR) (Monnier et al. 1999; Smith et al. 2001), the star's temperature would have to be extremely cool (2225 K!) to have such a large radius. Using *K*-band photometry and a simple model, Monnier et al. (2004) suggest an effective temperature of 2600 K, similar to the 2800 K value found by Le Sidaner & Le Bertre (1996); again, see discussion in Monnier et al. (1999, 2004). We note that none of these stellar properties are in accord with stellar evolutionary theory (Fig. 3*c*), and, indeed, based on its inferred mass-loss history, Humphreys et al. (2005) describe the star as "perplexing" and argue that it may be in a "unique evolutionary state." Such an object may provide important insight into a previously unrecognized avenue of normal stellar evolution, or its peculiarities may be the product of (for instance) binary evolution, as is the case for VV Cep. Smith et al. (2001) state that any hot, massive companion in VY CMa would have been previously detected spectroscopically, but we believe that further searching, particularly in the UV, is warranted. This star was not included in our sample, but we hope to perform an analysis in the near future.

3.4. *Comparison with* $(V-K)_0$

In § 3.2 we derived a precise relationship between spectral subtype and effective temperature based primarily on the strengths of the TiO band. One test of this result's accuracy is to check for consistency with other temperature indicators. Josselin et al. (2000) have emphasized the usefulness of *K*-band photometry in deriving bolometric luminosities of RSGs, as the BC to the *K* band is relatively insensitive to effective temperature and surface gravities, while RSGs themselves are less variable in the *K* band than at *V*. In addition, correction for interstellar reddening

[8] Also known as Herschel's "Garnet Star," this star is often cited as the largest known normal star; see http://www.astro.uiuc.edu/~kaler/sow/garnet.html.

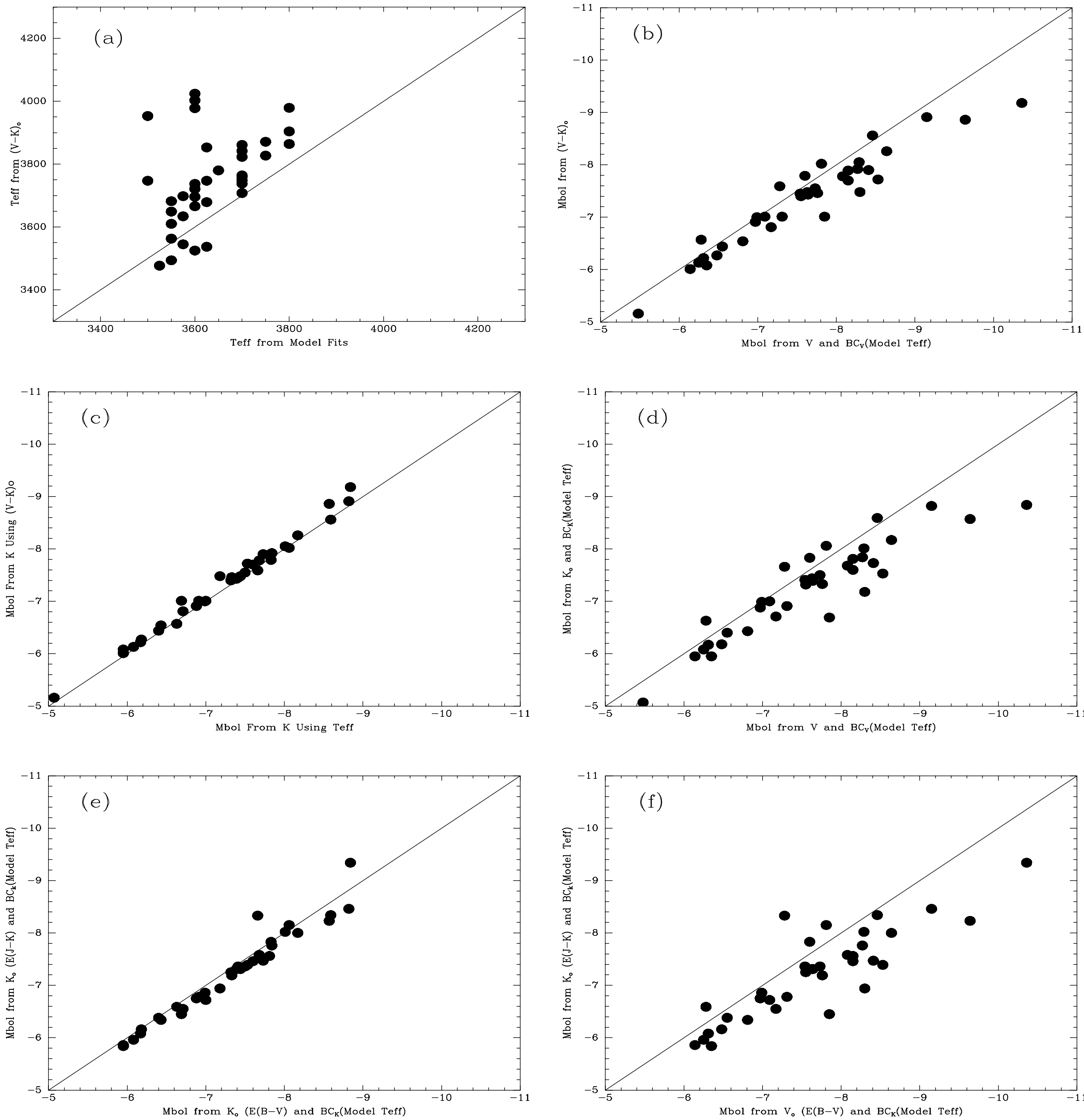

Fig. 5.—Derivation of the physical properties of RSGs based on K-band photometry. In (a) we compare the effective temperatures derived from $(V-K)_0$ with those found by fitting the models to our spectra. The line shows the 1:1 relationship. The $T_{\rm eff}$ values from the broadband color shows considerable scatter and an average offset of 100 K. However, in (b) we find excellent agreement between the bolometric luminosities $M_{\rm bol}$ derived from V and our effective temperatures and those derived from the $V-K$, in accordance with the expectation of Josselin et al. (2000), who note the usefulness of K in deriving $M_{\rm bol}$. In both (a) and (b) we restrict the sample only to stars with $(V-K)_0$ colors between 2.9 and 8.0, the "sensible range" over which our transformation equations are good. In (c) we demonstrate that deriving the bolometric luminosity from the $(V-K)_0$ colors agrees well with deriving it from K_0 with the BC at K coming from the model fits in the optical. In (d) we compare the bolometric luminosities derived from K_0 and the BC at K coming from the model fits in the optical with the bolometric luminosities derived purely from the optical fits. Again, the agreement is excellent for most stars, with a few outliers as noted in Table 4. Finally, in (e) and (f) we compare the bolometric luminosities at K using $E(J-K)$ vs. those derived from K (e) and V (f) using our $E(B-V)$ values. The two outliers in (e) are KY Cyg and KW Sgr, for which the $J-K$ colors result in luminosities intermediate between our V and K results.

is minor at K. At the same time, the effective temperature is a very sensitive function of $(V-K)_0$. Since over half our sample have K-band photometry (Table 1), we can perform some exacting tests of the models to see if we obtained similar physical parameters by very different techniques.

We have derived synthetic $(V-K)_0$ colors for our models following the procedure and assumptions of Bessell et al. (1998). The V bandpass comes from Bessell (1990), while the K bandpass comes from Bessell & Brett (1988). Note that the latter is similar to the "standard" K system of Elias et al. (1982) and

Johnson (1965), and a good approximation to the convolution of detector and filter used at the United Kingdom Infrared Telescope (UKIRT) and with most European Southern Observatory (ESO) and NOAO instrumentation; however, this differs considerably from the K_s filter employed in other modern instruments, such as the Two Micron All Sky Survey (2MASS) survey and the Very Large Telescope (VLT) Infrared Spectrometer and Array Camera (ISAAC) instruments, and the transformations given below do not apply to K_s.

We found that we could approximate the relationship between $(V-K)_0$ color as a simple power law:

$$T_{\rm eff} = 7741.9 - 1831.83(V-K)_0 + 263.135(V-K)_0^2 - 13.1943(V-K)_0^3 \text{ K},$$

over the range $2.9 < (V-K)_0 < 8.0$, (3200–4300 K) with a dispersion of 11 K, where the dispersion comes from considering the full range of appropriate surface gravities ($\log g = -1$ to 1); see Figure 4*a*. The BC at K is an almost linear relationship with effective temperature over the range $3200 \text{ K} < T_{\rm eff} < 4300$ K:

$$\text{BC}_K = 5.574 - 0.7589(T_{\rm eff}/1000 \text{ K}),$$

with a dispersion of 0.01 mag (Fig. 4). We have included these BC_K values in Table 6.

We dereddened the $V-K$ colors in Table 1, using the extinction values derived from the model fits and assuming $E(V-K) = 2.73E(B-V)$, based on Schlegel et al. (1998); this does not account for a modest change due to the shifts of the effective wavelengths of the bandpasses for very red stars. We compare the effective temperatures derived by this method with those obtained from the spectral types in Figure 5*a*. The scatter is large, as one might expect given the strong functional dependence of $T_{\rm eff}$ on $(V-K)_0$, the variability of V, and the fact that the effective temperatures now depend strongly on the assumed reddenings. Note that our uncertainty of 0.15 in A_V translates to an uncertainty of 0.13 in $E(V-K)$, and hence 50 K in $T_{\rm eff}$. However, in general the agreement is good, with the $(V-K)_0$ colors yielding a temperature whose median difference is 60 K warmer than our adopted scale.

How well do the bolometric luminosities then agree? In Figure 5*b* we show the relationship between the bolometric luminosities derived from V and our $T_{\rm eff}$ values (Table 4) and those found *purely from the dereddened $V-K$ colors*. The agreement here is excellent, with only one significant outlier, KY Cyg, the most luminous star shown.

What if instead we had derived bolometric luminosities without reference to the $V-K$ colors at all, but rather simply used the extinction values from the fits to derive the absolute magnitude in the K band [$M_K = K - 0.37E(B-V) - (m-M)_0$] and then determined the BC at K using the $T_{\rm eff}$ of the models fits? We give that comparison in Figure 5*c*. Clearly there is excellent agreement.

In Figure 5*d* we show the comparison between the bolometric magnitudes derived from the K band in the same manner as in Figure 5*c* and the bolometric magnitudes derived from the visible. This plot is similar to that of Figure 5*b*, with excellent agreement in general. There are five significant outliers, whose differences are greater than 1 mag using the two methods (KY Cyg, CD $-31°4916$, BD $+35°4077$, BD $+60°2613$, and HD 14528), all in the sense that the bolometric luminosity derived from V may be overly luminous. We flagged all five stars in Figure 3, as well as in Table 4.

The fact that these five outliers were all more luminous based on V than on K raised the question as to whether our method was systematically overestimating A_V. Recall that we did find that our A_V values tend to be higher than that of OB stars in the same clusters and associations. Following a suggestion offered by the referee, we derived the bolometric luminosities at K based instead on the $J-K$ colors alone, ignoring our A_V values. We used the effective temperatures derived from our model fits both to determine the BCs and to compute the intrinsic $(J-K)_0$ colors from a relationship we found using the MARCS models:

$$(J-K)_0 = 3.10 - 0.547(T_{\rm eff}/1000 \text{ K}).$$

We adopt the broadband extinction terms suggested by Schlegel et al. (1998), i.e., $A_K = 0.70E(J-K)$. Again, the numerical factor here does not take into account the shift of R_K due to the change in the effective wavelengths of the broadband filters, but it should be good enough for the test we intend. The $J-K$ photometry comes from Josselin et al. (2000) and references therein. We show this comparison between the two ways of deriving $M_{\rm bol}$ from K in Figure 5*e*. There is excellent agreement between the two methods. Thus, there cannot be anything systematically wrong with our A_V values in general. Interestingly, the two stars with the largest deviations in this figure are KY Cyg and KW Sgr. The $J-K$ correction suggests that if anything the $M_{\rm bol}$ values should be intermediate between what we derive above from V and from K using our values for the extinction and that perhaps our extinction values for these two stars are too low, rather than too high. A comparison between the luminosities derived from K and $E(J-K)$ and those derived from V and the extinctions derived from our model fits is shown in Figure 5*f*; this is very similar to what we found in Figure 5*d*.

We summarize the conclusions from these comparisons as follows. First, the MARCS models yield consistent results (to within 100 K) both from the molecular band strengths and from the $V-K$ colors. Thus if one's goal is simply to derive bolometric luminosities, V- and K-band data will suffice for most purposes, if one has an estimate of the reddenings. However, for accurate placement in the H-R diagram (requiring $T_{\rm eff}$), then there is as yet no substitute for spectroscopy and the use of molecular bands. It is possible that other colors, such as $V-R_{\rm C}$, might prove more effective in determining the effective temperatures than $V-K$, given the shorter baseline and therefore lower sensitivity to reddening, i.e., $E(V-R_{\rm C}) = 0.64E(B-V)$. We will explore this further when we consider the Magellanic Cloud sample, as these stars have simultaneous V and R measures and the reddenings are low and uniform (Massey et al. 1995).

4. CONCLUSIONS AND SUMMARY

We have determined a new effective temperature scale for Galactic RSGs by fitting moderate resolution (4–6 Å) spectrophotometry with the new MARCS stellar atmosphere models. Our effective temperature scale is significantly warmer than previous scales, particularly for the later M supergiants, for which the differences amount to 400 K. However, our new results give excellent agreement with the evolutionary tracks of Meynet & Maeder (2003), resolving the issue posed by Massey (2003) that the evolutionary models do not produce RSGs as cool and as luminous as "observed."

Our fitting showed excellent agreement between the models and data for the majority of the stars. The Ca I λ4226 and Ca II H and K atomic lines appear to be too strong in the models, but the molecular transitions agree well at this dispersion. When we compare the physical properties derived from the model fits to our optical spectrophotometry with those found from the models using only the dereddened $V - K$ colors, we find good agreement, providing an exacting demonstration of the self-consistency of the MARCS models.

Extension of these studies to the Magellanic Clouds is underway, which should help us understand the effect that metallicity has on the effective temperature scale of RSGs. In addition, the facts that the reddenings are small and uniform and the distances are known (van den Bergh 2000) will allow further investigation of colors as probes of the physical properties of these interesting massive stars.

This work was supported by NSF grant AST 00-093060 to P. M. and the NSF's Research Experience for Undergraduates program at Northern Arizona University (AST 99-88007). We are very grateful for the excellent hospitality and support provided by the staff at KPNO and CTIO and also thank Nat White and Kathy Eastwood for their encouragement and guidance. Hank Levesque pointed us toward some discussions of previous "record holders" of the largest stars known, and we also had correspondence with Jim Kaler on this topic. John Monnier kindly called his interesting results on VY CMa to our attention. We also gratefully acknowledge correspondence with Geoff Clayton. Comments by the referee, Roberta Humphreys, led to improvements in the presentation of our arguments in several places.

REFERENCES

Aller, L. H. 1960, in Stellar Atmospheres, ed. J. L. Greenstein (Chicago: Univ. Chicago Press), 232
Bauer, W. H., & Bennett, P. D. 2000, PASP, 112, 31
Becker, W., & Fenkart, R. 1971, A&AS, 4, 241
Bessell, M. S. 1990, PASP, 102, 1181
Bessell, M. S., & Brett, J. M. 1988, PASP, 100, 1134
Bessell, M. S., Castelli, F., & Plez, B. 1998, A&A, 333, 231
Bochkarev, N. G., & Sitnik, T. G. 1985, Ap&SS, 108, 237
Cardelli, J. A., Clayton, G. C., & Mathis, J. S. 1989, ApJ, 345, 245
Conti, P. S. 1988, in O Stars and Wolf-Rayet Stars, ed. P. S. Conti & A. B. Underhill (NASA SP-497; NASA: Washington, DC)
de Zeeuw, P. T., Hoogerwerf, R., de Bruijne, J. H. J., Brown, A. G. A., & Blaauw, A. 1999, AJ, 117, 354
Dyck, H. M., Benson, J. A., van Belle, G. T., & Ridgway, S. T. 1996, AJ, 111, 1705
Elias, J. H., Frogel, J. A., & Humphreys, R. M. 1985, ApJS, 57, 91
Elias, J. H., Frogel, J. A., Matthews, K., & Neugebauer, G. 1982, AJ, 87, 1029
Fernie, J. D. 1983, ApJS, 52, 7
Flower, P. J. 1975, A&A, 41, 391
———. 1977, A&A, 54, 31
Freytag, B., Steffen, M., & Dorch, B. 2002, Astron. Nach., 323, 213
Garmany, C. D., & Stencel, R. E. 1992, A&AS, 94, 211
Gustafsson, B., Bell, R. A., Eriksson, K., & Nordlund, Å. 1975, A&A, 42, 407
Gustafsson, B., Edvardsson, B., Eriksson, K., Mizuno-Wiedner, M., Jorgensen, U. G., & Plez, B. 2003, in ASP Conf. Ser. 288, Stellar Atmosphere Modeling, ed. I. Hubeny, D. Mihalas, & K. Werner (San Francisco: ASP), 331
Gustafsson, B., & Jorgensen, U. G. 1994, A&A Rev., 6, 19
Harris, G. J., Polyansky, O. L., & Tennyson, J. 2002, ApJ, 578, 657
Humphreys, R. M. 1970, AJ, 75, 602
———. 1978, ApJS, 38, 309
Humphreys, R. M., Davidson, K., Ruch, G., & Wallerstein, G. 2005, AJ, 129, 492
Humphreys, R. M., & McElroy, D. B. 1984, ApJ, 284, 565
Hutchings, J. B., & Wright, K. O. 1971, MNRAS, 155, 203
Jaschek, C., & Jaschek, M. 1987, The Classification of Stars (Cambridge: Cambridge Univ. Press)
Jennens, P. A., & Helfer, H. L. 1975, MNRAS, 172, 667
Johnson, H. L. 1964, Bol. Obs. Tonantzintla Tacubaya 3, 305
———. 1965, ApJ, 141, 923
———. 1966, ARA&A, 4, 193
Johnson, H. L., Iriarte, B., Mitchell, R. I., & Wisniewskj, W. Z. 1966, Comm. Lunar Planet. Lab., 4, 99
Josselin, E., Blommaert, J. A. D. L., Groenewegen, M. A. T., Omont, A., & Li, F. L. 2000, A&A, 357, 225
Josselin, E., Plez, B., & Mauron, N. 2003, in IAU Symp. 210, Modelling of Stellar Atmospheres, ed. N. Piskunov, W. W. Weiss, & D. F. Gray (San Francisco: ASP), F9
Kurucz, R. L. 1992, in IAU Symp. 149, The Stellar Populations of Galaxies, ed. B. Barbuy & A. Renzini (Dordrecht: Kluwer), 225
Lee, T. A. 1970, ApJ, 162, 217
Le Sidaner, P., & Le Bertre, T. 1996, A&A, 314, 896
Massey, P. 1998, ApJ, 501, 153
———. 2003, ARA&A, 41, 15
Massey, P., Lang, C. C., DeGioia-Eastwood, K., & Garmany, C. D. 1995, ApJ, 438, 188
Massey, P., & Olsen, K. A. G. 2003, AJ, 126, 2867
Massey, P., Plez, B., Levesque, E. M., Olsen, K. A. G., Clayton, G. C., & Josselin, E. 2005, ApJ, submitted
McCall, M. L. 2004, AJ, 128, 2144
Mel'Nik, A. M., & Efremov, Y. N. 1995, Pis'ma Astron. Zh., 21, 13
Mermilliod, J. C., & Paunzen, E. 2003, A&A, 410, 511
Meynet, G., & Maeder, A. 2003, A&A, 404, 975
Moitinho, A., Emilio, J., Yun, J. L., & Phelps, R. L. 1997, AJ, 113, 1359
Monnier, J. D., Tuthill, P. G., Lopez, B., Cruzalebes, P., Danchi, W. C., & Haniff, C. A. 1999, ApJ, 512, 351
Monnier, J. D., et al. 2004, ApJ, 605, 436
Morgan, W. W., & Keenan, P. C. 1973, ARA&A, 11, 29
Nicolet, B. 1978, A&AS, 34, 1
Partridge, H., & Schwenke, D. W. 1997, J. Chem. Phys., 106, 4618
Perrin, G., Ridgway, S. T., Coude du Foresto, V., Mennesson, B., Traub, W. A., & Lacasse, M. G. 2004, A&A, 418, 675
Plez, B. 2003, in ASP Conf. Ser. 298, *GAIA* Spectroscopy: Science and Technology, ed. U. Munari (San Francisco: ASP), 189
Plez, B., Brett, J. M., & Nordlund, Å. 1992, A&A, 256, 551
Richards, A. M. S., Yates, J. A., & Cohen, R. J. 1998, MNRAS, 299, 319
Ruprecht, J. 1966, Trans. IAU, 12B, 350
Sagar, R., & Joshi, U. C. 1981, Ap&SS, 75, 465
Saito, M., Sato, H., Saijo, K., & Hayasaka, T. 1980, PASJ, 32, 163
Schaller, G., Schaerer, D., Meynet, G., & Maeder, A. 1992, A&AS, 96, 269
Schlegel, D. J., Finkbeiner, D. P., & Davis, M. 1998, ApJ, 500, 525
Smith, N., Humphreys, R. M., Davidson, K., Gehrz, R. D., Schuster, M. T., & Krautter, J. 2001, AJ, 121, 1111
Tsuji, T. 1986, ARA&A, 24, 89
van den Bergh, S. 2000, The Galaxies of the Local Group (Cambridge: Cambridge Univ. Press)
White, N. M., & Wing, R. F. 1978, ApJ, 222, 209
Wright, K. O. 1977, JRASC, 71, 152
Young, J. S., et al. 2000, MNRAS, 315, 635